POLITECNICO DI TORINO
Repository ISTITUZIONALE

The effectiveness of different wear indicators in quantifying wear on railway wheels of freight wagons

Original
The effectiveness of different wear indicators in quantifying wear on railway wheels of freight wagons / de Paula Pacheco, P.A., Magelli, M., Lopes, M.V., Correa, P.H.A., Zampieri, N., Bosso, N., dos Santos, A.A.. - In: RAILWAY ENGINEERING SCIENCE. - ISSN 2662-4745. - ELETTRONICO. - 32:(2024), pp. 307-323. [10.1007/s40534-024-00334-8]

Availability:
This version is available at: 11583/2990399 since: 2024-07-05T12:39:28Z

Publisher:
Springer

Published
DOI:10.1007/s40534-024-00334-8

Terms of use:

This article is made available under terms and conditions as specified in the corresponding bibliographic description in the repository

Publisher copyright

(Article begins on next page)

19 November 2026

Railway Engineering Science (2024) 32(3):307–323
https://doi.org/10.1007/s40534-024-00334-8

The effectiveness of different wear indicators in quantifying wear on railway wheels of freight wagons

Philipe Augusto de Paula Pacheco[1,2] · M. Magelli[3] · Matheus Valente Lopes[2] · Pedro Henrique Alves Correa[2] · N. Zampieri[3] · N. Bosso[3] · Auteliano Antunes dos Santos[2]

Received: 25 October 2023 / Revised: 23 January 2024 / Accepted: 4 February 2024 / Published online: 9 April 2024
© The Author(s) 2024

Abstract
Railway infrastructure relies on the dynamic interaction between wheels and rails; thus, assessing wheel wear is a critical aspect of maintenance and safety. This paper focuses on the wheel–rail wear indicator T-gamma ($T\gamma$). Amidst its use, it becomes apparent that $T\gamma$, while valuable, fails to provide a comprehensive reflection of the actual material removal and actual contact format, which means that using only $T\gamma$ as a target for optimization of profiles is not ideal. In this work, three different freight wagons are evaluated: a meter-gauge and a broad-gauge heavy haul vehicles from South American railways, and a standard-gauge freight vehicle operated in Europe, with different axle loads and dissimilar new wheel/rail profiles. These vehicles are subjected to comprehensive multibody simulations on various tracks. The simulations aimed to elucidate the intricate relationship between different wear indicators: $T\gamma$, wear index, material removal, and maximum wear depth, under diverse curves, non-compensated lateral accelerations (A_{nc}), and speeds. Some findings showed a correlation of 0.96 between $T\gamma$ and wear depth and 0.82 between wear index and material removed for the outer wheel. From the results, the $T\gamma$ is better than the wear index to be used when analyzing wear depth while the wear index is more suited to foresee the material lost. The results also show the low influence of A_{nc} on wear index and $T\gamma$. By considering these factors together, the study aims to improve the understanding of wheel–rail wear by selecting the best wear analysis approaches based on the effectiveness of each parameter.

Keywords Wear index · Wear volume · Wear modeling · Dynamic simulation

1 Introduction

To maximize the performance of their operations, freight, passenger, and heavy haul railways continue to increase axle loads and speeds [1]. Consequently, those severe wheel–rail (W/R) contacts generate increasing wear, leading to more intense changes in the wheel profile [2]. Wheel transversal profiles significantly impact vehicle dynamic behavior as worn and damaged profiles can adversely affect vehicle traction and braking operations, while threatening running stability and safety, increasing the risk of derailment [3]. Therefore, there is a strong interest in developing approaches and methodologies for designing optimal slow-wear wheel profiles [4].

Two semi-empirical approaches are commonly used to model wear processes according to [5]. The first approach relates material loss to energy in contact using the $T\gamma$ wear number. The second approach uses tribological models of material removal integrated with multibody dynamics simulations. Elkins and Eickhoff [6] first defined $T\gamma$ as the dot product of creep force and creepage based on experimental work. This work has shown that the amount of metal removed through wear is proportional to the energy expended in the W/R contact [5, 7]. Krishna et al. [8] studied global methods employing $T\gamma$ and shakedown map, and local methods such as the KTH model and Wedge models

✉ Philipe Augusto de Paula Pacheco
philipe.pacheco@ifsudestemg.edu.br

[1] Federal Institute of the Southeast of Minas Gerais (IF Sudeste MG), Técnico Panamá Street 45, Santos Dumont, MG 36246-311, Brazil

[2] Railway Laboratory (Lafer), Universidade Estadual de Campinas (UNICAMP), Mendeleyev Street 200, Campinas, SP 13083-872, Brazil

[3] Department of Mechanical and Aerospace Engineering, Politecnico Di Torino, C.so Duca degli Abruzzi 24, 10129 Turin, Italy

to quantify rolling contact fatigue (RCF). The authors found that damage increments are significantly lower and concentrated in lower $T\gamma$ regions. The curve radius is directly proportional to $T\gamma$, as expected. Energy dissipation, $T\gamma$ values, are highest for flange contact cases. Currently, several models are attempting to quantify wear using the wear index ($T\gamma/A$). The wear index is defined as the energy expended per unit distance traveled calculated for each wheel–rail contact, where A is the wheel–rail contact patch area [7, 9, 10]. There are other less commonly used wear models, such as the wear concentration index (WCI) proposed by Ye and Hecht [11]. WCI is based on statistical distributions of lateral contact positions and wear rates over the wheel profile.

When solving W/R optimization problems, it is common to represent the wear index as an objective function and minimize it [12]. Usually, $T\gamma$ is used as an indicator of optimization, due to its low computational cost. According to Ye and Hecht [11], this approach, however, faces some issues. First, the wear rate is not proportional to the wear number ($T\gamma$), which implies that a small $T\gamma$ does not necessarily mean a small material loss. Second, a small $T\gamma$ value suggests that wheel–rail contact is likely to occur in the wheel tread. The optimized wheel profile focused on minimal $T\gamma$ value, therefore, may result in a concentrated distribution of wheel–rail contact points around the nominal rolling circle, accelerating hollow wear. This indicates that simply using the $T\gamma$ value as the optimization target cannot guarantee that the wheel profile will show excellent wear performance during long-term service [13].

These limitations can be evaluated by considering worn profiles through wear simulations [11, 12]. There are several numerical models to calculate wheel wear. In multibody software, such as SIMPACK ® or VAMPIRE ®, advanced wheel–rail contact models are used to analyze vehicle behavior and wheel–rail wear [14]. One of the most common strategies involves iterating dynamic simulations with updated profiles [3]. The Archard wear equation, which states that wear is proportional to normal force, sliding distance and inversely to material hardness, is one of the most used in works on wear [5, 12, 15]. An accurate solution can be obtained with this method, but it is time-consuming.

To evaluate the effectiveness of the $T\gamma$ and wear index in quantifying wear on railway wheels, the present work compares the $T\gamma$ values with the wear index magnitude, based on wear area and wear depth obtained with dynamic vehicle on-track simulations. To extract general information, this paper considers freight wagons used in different countries (Brazil and Italy) and running on tracks with different gauges. The analysis is limited to freight wagons as this type of vehicle relies on standard bogie architectures, such as the three-piece bogie and Y25 bogie, which are the bogie types considered in this paper for the Brazilian and European wagons respectively. The relationship between wear indicators and worn material is investigated considering short-run simulations with new profiles, assuming that the level of wear of the profiles does not strongly affect the effectiveness of the wear indicators in estimating wear. A description of the research methodology is provided in Sect. 2, including details about multibody simulations and wear calculations. The results are discussed in Sect. 3, while conclusions on findings are presented in Sect. 4.

2 Methods

In the railway industry, multibody dynamic software is widely used to study train/track interaction. SIMPACK® software is one of the most used because of its flexibility and coverage, since it cannot only simulate passenger and freight trains, including locomotives, but also small components and the wheel–rail wear, allowing dynamic analysis through its post-processing system [16].

The process of comparison between $T\gamma$ and wear index started with the development of multibody dynamic simulations with three different wagons, two American bogies widely used in Brazilian railways, with meter and broad gauge, and a European bogie with standard gauge running in Italy. The wagons were chosen to verify the generality of the results obtained. The output of the simulation is the wear number ($T\gamma$), wear index ($T\gamma/A$), wear depth, and wear area. The results for these variables are sent to a code in MATLAB® where they are processed.

In this section, the dynamic models are presented, focusing on the wear analysis. The section is organized as follows: The dynamics models of the wagon using the commercial software SIMPACK® are given in Sec. 2.1. Section 2.2 presents the parameters used in this study, like curves, rail cant, speed, wheel profiles, etc. Finally, in Sec. 2.3, the wear analysis for both freight railways in Brazil and in Italy are presented.

2.1 Dynamic model

For all models, the Discrete Elastic Contact method [17] was used to guarantee a more faithful representation of the contact. This is the semi-Hertzian contact method provided by SIMPACK®. Normal and tangential forces are calculated based on the actual contact patch shape. The tangential way to obtain forces is similar to FASTSIM. This method differs from conventional methods in that all input quantities, such as creepages, creep reference velocities, normal pressures, and curvatures, are determined locally within a single discrete slice. For actual elliptic contact patches, the FASTSIM results are consistent [18].

In all simulations, the wagon speed profile is kept essentially constant along the track. This is achieved by applying

a traction force acting between the vehicle carbody and a follow track marker, i.e., a marker defined on the track which follows the position of a reference body joint. The traction force only acts in the longitudinal direction so that it does not provide the lateral forces that may affect the contact point position in the lateral direction. The traction force F_t is calculated in each time-step t with a proportional controller, giving a force magnitude which is proportional to the deviation of the actual wagon speed v_w from the reference speed v_{ref}, using a proportionality constant K_p:

$$F_t(t) = K_p\left[v_{ref} - v_w(t)\right]. \quad (1)$$

The proportionality constant was finely tuned to ensure a stable speed along the track in all simulations without leading to numerical instabilities or abnormal peaks in the longitudinal force. This approach gives results strongly consistent with the application of a driven joint with constant velocity on the carbody, but also allows to simulate the effect of a tractive force on the wagon connection system. In future studies, the approach chosen can be upgraded to consider a more refined model of the coupling elements on both Brazilian and European wagons.

2.1.1 Brazilian railway wagons

The Brazilian railway has an essential fleet of gondola wagons GDE and GDT—Ride Control wagons, meter gauge (1.0 m) and broad gauge (1.6 m), respectively. A wagon with two bogies of each type was modeled. The simulation model of the wagons has been built and validated in previous works [19–23].

The ride control bogie is a three-piece bogie. The loaded axle weight for GDT is 31.5 t, thus the wagon is considered a heavy-haul freight car. The GDE loaded axle weight is 27.5 t. The Ride Control bogie model is shown in Fig. 1a.

In the primary suspension, the wheelset bearing is coupled to the side frame pedestal by a rubber PAD adapter [25]. In the multibody model, this element was represented as three connection elements expressing vertical, lateral, and longitudinal stiffness and damping. All three elements are aligned, and the middle element features non-linear longitudinal and lateral stiffness characteristics.

Another defining characteristic of this bogie is its secondary suspension. In addition to the spring system, a wedge with constant damping was added. The dry friction between wedge contact surfaces was modeled using discrete contact elements.

This type of bogie also uses roller side bearings. Since the type of balance support modeled is not of constant contact, the contact model of the roller side bearing was made with a spring (bushing type).

2.1.2 European wagon

The reference European wagon is a freight wagon equipped with the Y25 bogie; the typical bogie used by railway freight wagons running on European lines. Since many different types of freight wagons can run on Italian lines, the selected vehicle is a Talns wagon, having a length over buffers of 10.53 m and a bogie spacing of 6.1 m, with both values close to the ones of the Brazilian wagon, but with a lower axle-load of 16.4 t. The model is built starting from an existing validated SIMPACK® model of the Y25 bogie, described in [24] and shown in Fig. 1b. The model includes four wheelset bodies, eight axle-box bodies, two rigid bogie frame bodies, and two half carbodies. All bodies have 6 degrees of freedom (DOFs), defined via the general rail track joint available in SIMPACK®, except for the axle boxes, which are only allowed to rotate with respect to the corresponding wheelset. The reference profiles are the wheel S1002 profile and the UIC60 rail profile with a 1:20 cant angle.

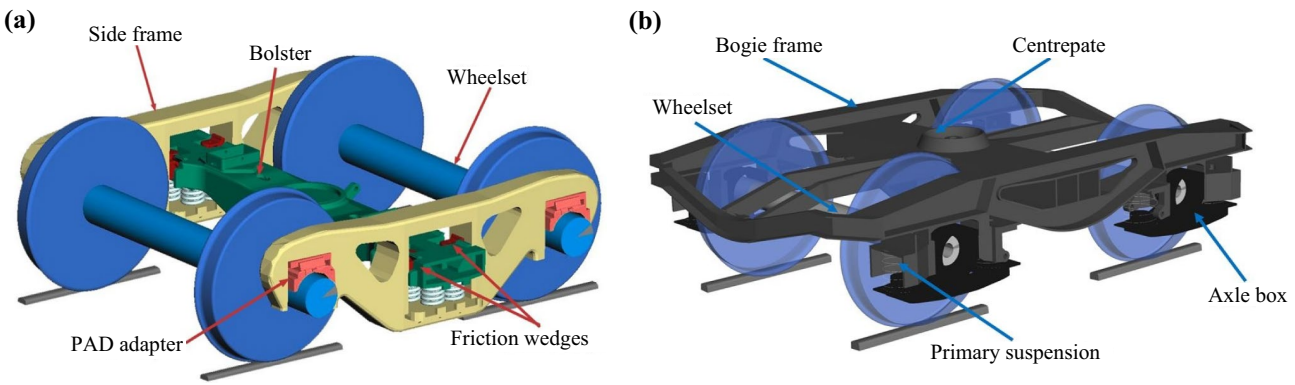


Fig. 1 Models of **a** Ride Control bogie (BR) [19] and **b** Y25 bogie (EU) [24] in SIMPACK®

The model considers all nonlinearities of the primary suspension stage of the Y25 bogie, which includes a bilinear stiffness, thanks to load helical springs that only react when the payload of the wagon is above a threshold value, and the Lenoir link system for friction damping. The bilinear stiffness is modeled via the definition of a shear spring element with variable vertical stiffness, while the Lenoir link system is modeled with stick–slip 2D friction elements. The model of the Lenoir link also accounts for the bumpstop effect between the axle box and axle guard in both directions along the longitudinal axis.

The secondary suspension connecting the bogie frame to the carbody includes a spherical center plate and side bearers to limit the roll angle. The center plate is modeled with a bushing element that provides zero rotational stiffness and with expression elements for the estimation of the friction torques. On the other hand, the side bearers are modeled with a combination of linear spring-damper elements and expression elements for the calculation of the friction forces. Finally, to model the carbody roll stiffness, the two half carbodies are connected with a bushing element featuring high stiffness in all directions except for roll, where the total roll stiffness of the carbody is adopted.

2.2 Wear analysis

Wear number ($T\gamma$) is estimated through energy dissipation in the contact patch [23, 26]. The wear number is the product of the tangential force and creepage, shown in Eq. (2) [3].

$$T\gamma = |F_x v_x| + \left|F_y v_y\right| + |M_z \varphi_z|, \tag{2}$$

where F_x, F_y, and M_z are the longitudinal force, lateral force, and spin moment on the contact area, while v_x, v_y, and φ_z are the longitudinal, lateral, and spin creepage, respectively. Although SIMPACK® calculates $T\gamma$ without the spin part, we use the complete form of Eq. (2) in our analysis.

As already mentioned, wheel–rail wear is typically predicted using wear coefficient methods, such as the wear index ($T\gamma/A$), where A is the contact area [27]. Wear indexes are based on the proportional wear work done at the wheel/rail contact [28].

SIMPACK® simulation environment allows parallel and discrete wheel wear calculation, from which we can obtain the wear depth and wheel wear profile [12]. Archard's method was used to calculate wear since it is widely used in this field [29]. The wear volume V in m^3 is proportional to the sliding distance Δs in m and the normal force N in N, and inversely proportional to the hardness of the material, H in Pa:

$$V = \frac{N\Delta s}{H}k, \tag{3}$$

where k is a non-dimensional wear coefficient that depends on the contact pressure and slip velocity and is typically evaluated from experimental maps [30, 31]. The map adopted in this work is shown in Fig. 2, and the wear coefficients are extracted as the lowest values suggested by SIMPACK® documentation in each region. It is important to remark that the wear module implemented in SIMPACK® can estimate the wear depth distribution along the contact patch from the global volume calculated with Eq. (3); so the final worn profile shape can be obtained, but no information about this point is given in the documentation, because of intellectual property reasons. Nonetheless, the authors of the present paper found in previous activities that when using the equivalent elastic method, SIMPACK® spreads the worn volume proportionally to the Hertzian contact pressure [32].

2.3 Design of experiments

This study defined a set of tracks to generate different track conditions (Table 1). The reference track is composed of a straight Sect. (100 m), an entry curve transition (160 m) defined as a linear clothoid equation, a full curve to the left (200 m in length), an exit curve transition (160 m), then the same sequence to the opposite side, and a straight Sect. (100 m) to end (see Fig. 3). The differences between the tracks remain on the curve radius and cant angle, defined as a combination of speed and superelevation. The track features no external excitation hence no irregularities. Irregularities are neglected in this paper to avoid the effect of stochastic parameters in the evaluation of the relationship between wear indicators, under the assumption that irregularities should not impact the effectiveness of the indicators in estimating wear.

The three models in this study were subject to the same track at different speeds to gain negative, neutral, and

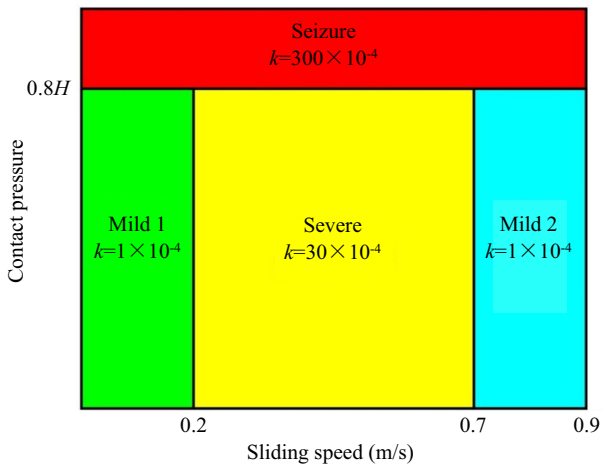


Fig. 2 Wear map used in the paper (adapted from Ref. [30])

Table 1 Runs description

Track	R (m)	V_{max} (km/h)	H/G (mm/m)	V_1 (km/h)	A_{nc1} (m/s^2)	V_2 (km/h)	A_{nc2} (m/s^2)	V_3 (km/h)	A_{nc3} (m/s^2)
1	300	77	100.0	49	−0.36	60	−0.06	78	0.58
2	500	100	100.0	64	−0.35	78	−0.04	100	0.56
3	750	112	75.0	62	−0.34	82	−0.04	110	0.51
4	1000	117	50.0	46	−0.33	78	−0.02	117	0.57
5	2000	166	50.0	65	−0.33	110	−0.02	120	0.07
6	300	64	50.0	32	−0.23	42	−0.04	64	0.57
7	500	83	50.0	41	−0.23	55	−0.02	83	0.57
8	750	96	37.5	38	−0.22	58	−0.02	96	0.58
9	1000	104	25.0	20	−0.21	55	−0.01	104	0.59
10	2000	147	25.0	29	−0.21	77	−0.02	120	0.31
11	300	48	0.0	30	0.23	40	0.41	48	0.59
12	500	62	0.0	30	0.14	45	0.31	62	0.59
13	750	76	0.0	35	0.13	50	0.26	76	0.59
14	1000	88	0.0	40	0.12	60	0.28	88	0.60
15	2000	125	0.0	60	0.14	80	0.25	120	0.56

Note: R is curve radius, H superelevation, G gauge, and V velocity

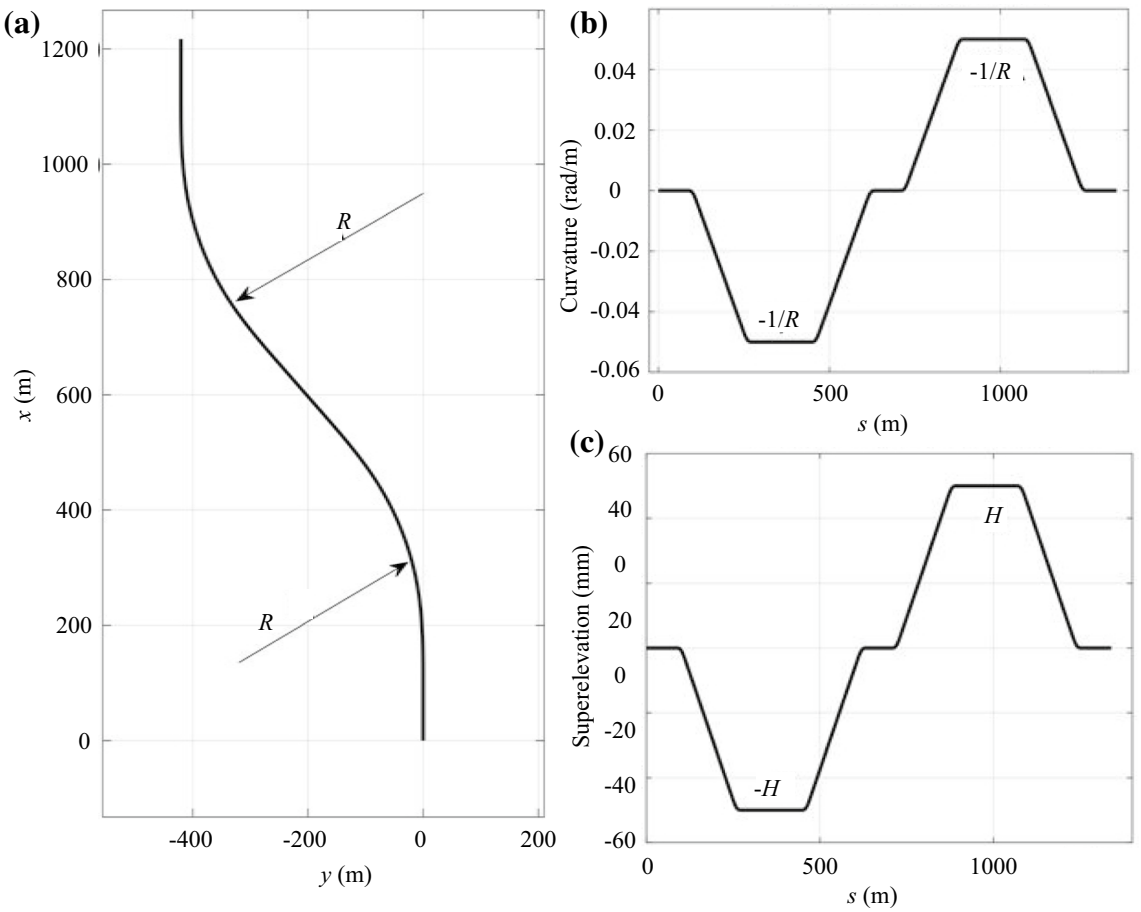


Fig. 3 An example of the designed **a** track layout, **b** curvature, and **c** superelevation

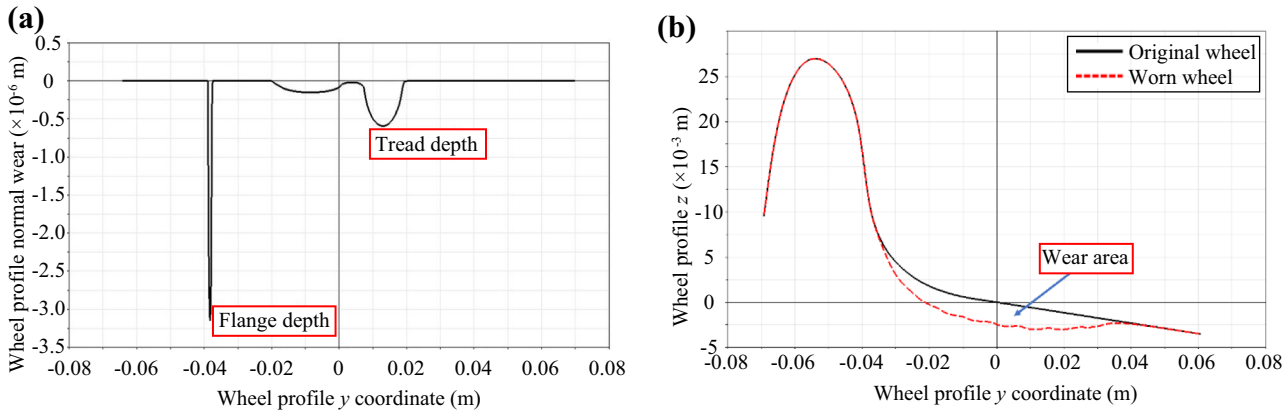


Fig. 4 Wear results: **a** normal wear; **b** wear area

positive non-compensated accelerations. Based on the ABNT 16810 [33] and the Italian railway administration (RFI) prescriptions 15/2016 [34], the non-compensated accelerations (A_{nc}) were limited and the theoretical values for each track set are shown in Table 1. The minimum curve radius considered in this paper is 300 m, as tighter curves are uncommon on Brazilian freight railways. Furthermore, when the curve radius is below 300 m, the gauge is typically widened on European lines, while Brazilian lines do not apply gauge widening, which would make it difficult to perform a fair comparison between European and Brazilian wagons. At the same time, tight curves are commonly characterized by lubrication at the wheel–rail contact interface, which changes the contact conditions. Therefore, modeling lubrication on tight curves would lead to a difficult interpretation of the wear results for curves with different radii, observing that this paper aims to investigate the effects due to vehicle dynamics rather than those related to the conditions of the wheel–rail contact interface.

When the simulation is complete, it is necessary to define the location and how the data should be collected. The wear number and wear index are selected as the integral average in the full region of the curve. The values of interest were collected on the wheels of the first wheelset, which features the highest wear.

SIMPACK® calculates wear based on the W/R contact region and applies it along the wheel profile contour according to contact positions and situations during simulation. An important result channel is normal wear, the amount of wheel material removed in normal direction to the profile at the respective lateral position y. The wear depth used in this work is calculated as the maximum normal wear (Fig. 4a). SIMPACK® also provides the vertical positions of the discrete profile points for the worn wheel profile. Using the original wheel profile and the worn wheel profile, the wear area can be calculated as the integral of the difference of the original and the worn profile vertical coordinates (Fig. 4b).

The wear depth and wear area are collected for the right wheel of the first wheelset and accumulated in the total length of each curve. In this study, the wear depth and wear area are related to the flange and tread regions, delimited by EN 13715 [35] and AAR M-107 [36]. For the European and Brazilian wheel profiles, the connection between the wheel tread and the flange zone starts at –26 mm and –23,7 mm from the tape line, respectively (Fig. 5).

One of the strengths of MBD software is the possibility to automate actions on the model and post-processing operations through scripting, i.e., by developing routines that can be called with external software [37]. We used an external MATLAB® code that calls QtScript and QSA routines from batch. The former modifies the model inputs and runs the simulations (Model and Solver scripting), while the latter is implemented to perform post-processing tasks (Post scripting).

3 Results and discussions

We used the correlation matrix to express the relation between the parameters obtained from all simulations (Fig. 6). The correlations were calculated according to the Pearson's equation [38]. For the outer wheel, the figure shows a remarkably high correlation (0.96) between $T\gamma$ and wear depth for. There is also a positive high correlation between the wear index and wear depth (0.92). This result indicates that the $T\gamma$ is a better index to use when analyzing wear depth than the wear index. As the $T\gamma$ value decreases, wheel–rail contact has a more concentrated distribution around the nominal rolling circle, increasing wear depth while reducing contact area [11]. $T\gamma$ and wear area presented a correlation of 0.79, while wear index and wear area presented 0.82. This way, the wear index has shown to be better than the $T\gamma$ to analyze the material removed due to wear. There is also a moderate correlation between $T\gamma$ of the inner

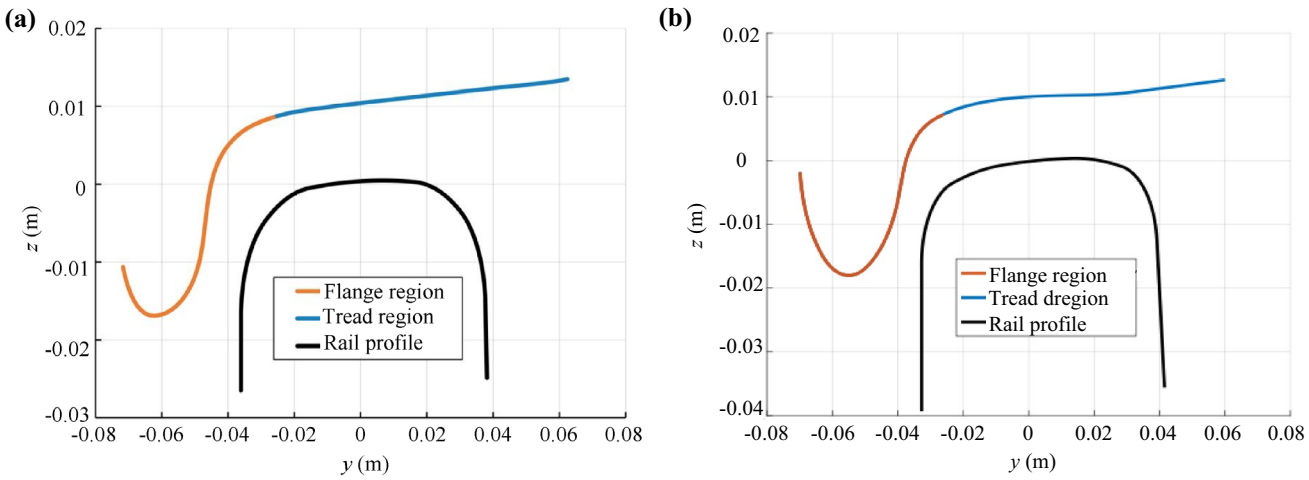


Fig. 5 Wheel and rail profiles with flange and tread regions: **a** GDT and GDE wagons; **b** European wagon

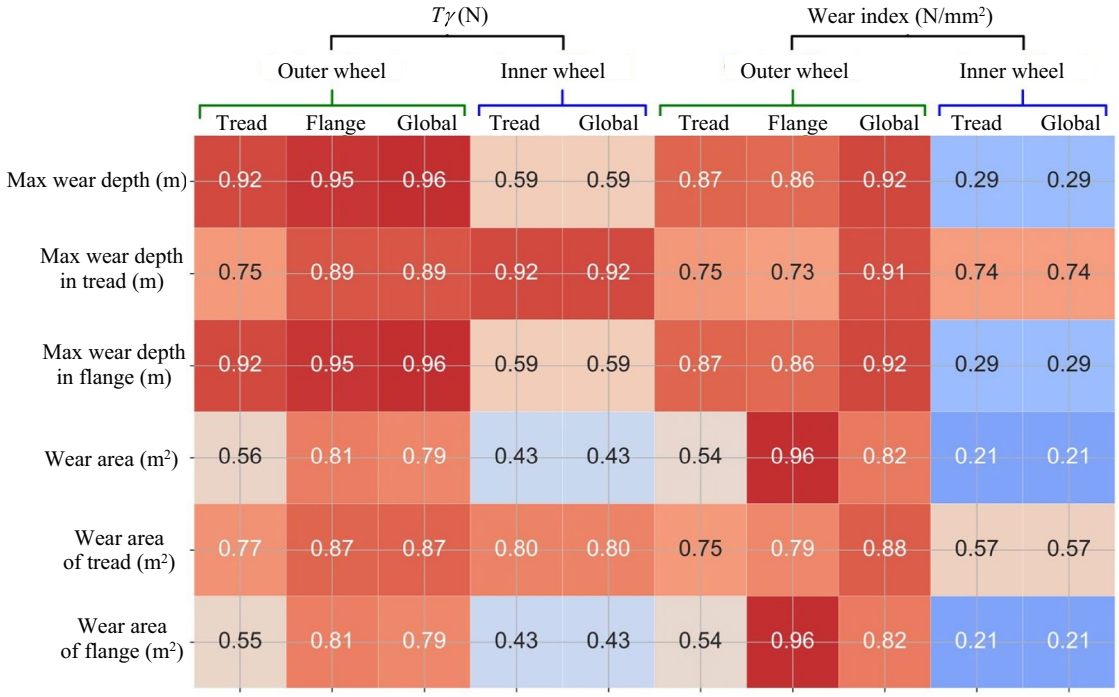


Fig. 6 Correlation matrix from all simulations

wheel and wear depth and wear area. A weak relationship was found between the wear index of the inner wheel and wear depth, and the wear index of the inner wheel and wear area. In short track simulations such as the present work, the influence of the internal wheel becomes less relevant, and a poorer correlation is observed on the inner wheel. As the external wheels receive the most effort on curves, they have the highest wear indicators and remove the most material. Especially when you have flange contact. The guidelines for interpreting the correlation coefficient were taken from [39]. Values between 0 and 0.3 indicate a weak relationship, between 0.3 and 0.7 a moderate relationship, and between 0.7 and 1.0 a strong relationship.

Figure 7 shows the outer wheel wear depth on the tread results. In Fig. 7a it is possible to see that $T\gamma$ increases as the curve radius decreases. The highest values of $T\gamma$ are observed for the broad-gauge wagon, followed by the meter and then the standard gauge. However, similar maximum wear depth values were observed for standard and meter gauge wagons. Furthermore, the Brazilian wagons, broad

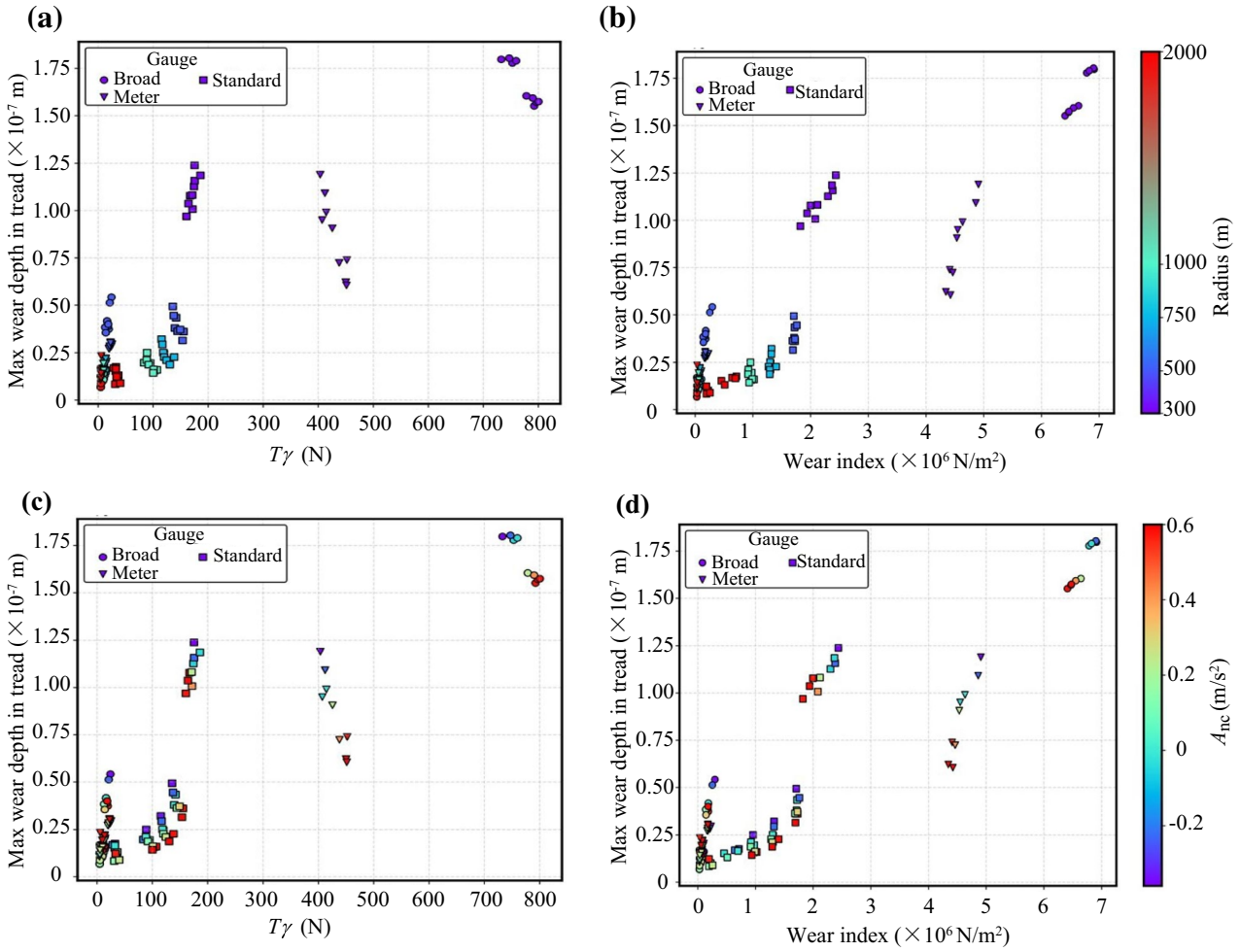


Fig. 7 Outer wheel wear depth on the tread: **a** by wear number and radius; **b** by wear index and radius; **c** by wear number and A_{nc}; **d** by wear index and A_{nc}

and meter-gauge, present two distinguish regions, where a high difference in the $T\gamma$ is observed; this happens due to the flange contact in the curves with a small radius, 300 m. A similar behavior is observed for the wear index (Fig. 7b). A positive correlation is observed between wear depth and wear index, while $T\gamma$ shows a negative correlation. In Fig. 6, it is possible to see that the wear index and wear depth correlation for the tread is 0.91 while 0.89 for the $T\gamma$ and wear depth.

Figure 7c and d show the results by A_{nc}. There seems to be a small influence of the A_{nc} in $T\gamma$ and wear index. A high negative influence in the wear depth is observed, i.e., an increase in the A_{nc} decreases the wear depth. Positive A_{nc} values mean that the wheelset will displace laterally to the field side; in sharp curves this can generate flange contact, reducing the tread forces and consequently the tread wear.

Figure 8 shows the contact overview for the Brazilian and European wagons. The Brazilian W/R contact points on the tread are more evenly spread as compared to the European profiles, this can accelerate the wear of the wheel for the Italian case. The jump of the contact point and larger distances between the contact points observed in the European contact (Fig. 8b) can result in the unstable behavior of the wheelset [40]. Figure 7 showing the results for the wear depth on the tread confirm indeed that the wear depth of the European wagons is comparable with the values recorded for the Brazilian wagons, despite the lower axle-load. Figure 8 highlights that for the Brazilian case, the W/R contact points can be either on the wheel flange or tread, while for the European profiles, additional contact points can be generated at the wheel flange-tread transition zone. However, the SIMPACK® routines for contact detection can deal with any number of contact points. Precisely, concerning the outer wheel in the full-curve section, for the Brazilian wagon a single contact point is detected on the tread in all curves except for the 300 m radius curve, whereby a single contact point is obtained on the flange and on the tread. On the other hand, for the European case, a single contact

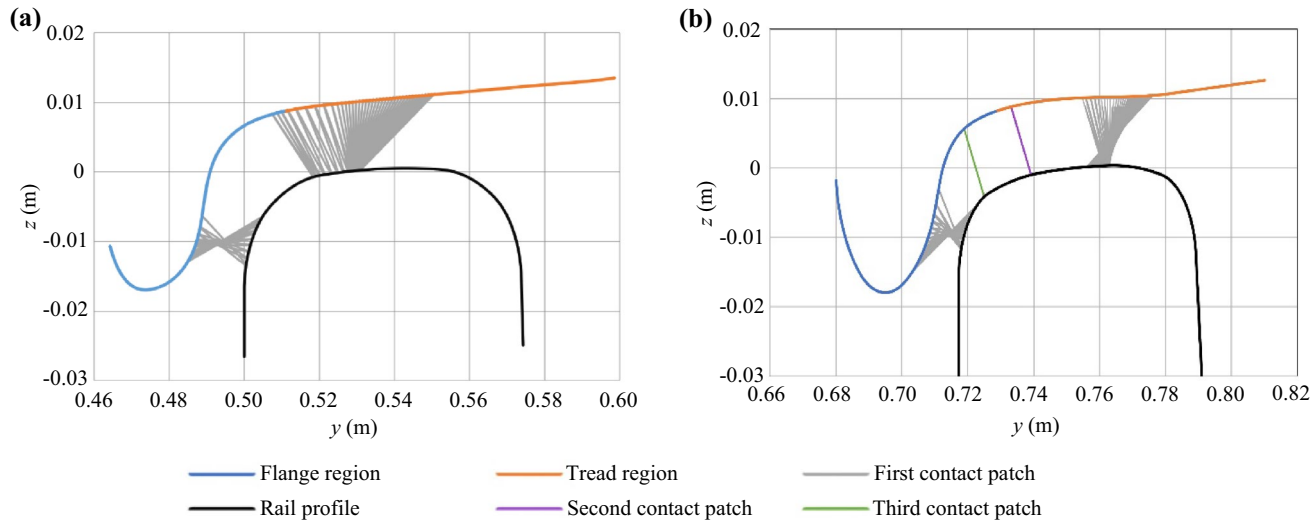


Fig. 8 Contact overview: **a** meter gauge (BR); **b** standard gauge (EU)

point is detected on the flange in the tightest curves, while an additional contact point is detected on the tread in the widest curves. Finally, for the intermediate curves, the SIMPACK® routines identify a third contact point in the flange-tread transition zone.

The results for the outer wheel wear depth on the flange are shown in Fig. 9. As for the tread, the $T\gamma$ and the wear index increase with the decrease of the curve radius. Besides that, the wear depth also increases with the $T\gamma$ and wear index. The Brazilian wagons show the highest values. Different from the tread results, the $T\gamma$ presents a positive correlation with the wear depth for the flange, while the wear index, a negative.

It is worth noting that points with a higher wear index correspond to points with a high negative A_{nc} whilst points with cant deficiency (higher positive A_{nc}) present a slightly smaller wear index. An excessively deficient superelevation on the small radius curve can result in a reduction of the contact area and, thus an increase in the wear index, although none of the simulations were close to derailment.

Nevertheless, the observed negative correlation in Fig. 9d, for the 300-m curve (only with flange contact for the meter gauge and the broad gauge wagons) doesn't follow the expected behavior. This is due to the calculation method for the total wear index, considered in this work, taking the sum of $T\gamma$ on the tread and the flange, divided by the sum of the contact areas, derived from the wear indices for tread and area. This way, the total wear index is weighted by the contact areas and, because the tread contact area is higher than the flange area, simulations with higher flange contact, hence higher wear depth in the flange, will be weighted by the flange area and will generate smaller wear indices, even though presenting the highest wear depths on the flange. We note that some analysis excludes the 300-m curve, and this calculation method does not impact the results. This total wear index method would be asserted in future wear works including narrow curves, to determine the most effective way to weight wear index for total calculation.

Also, the $T\gamma$ presents a better correlation with the Wear depth as can be seen in Fig. 5. For the Brazilian models, except for the results from the 300 m curve, the results are concentrated in a region with lower values of $T\gamma$, under 200 N, while for the Italian model, all results are under 200 N, making it difficult to draw any conclusions. This is because for the European wagon, all curves feature a contact point on the flange on the outer wheel, while for the Brazilian wagons, the contact point on the flange is obtained only for the 300 m radius curves. Therefore, it becomes important to analyze the results separating the data from the 300 m curve.

Figure 10 shows the outer wheel wear depth on the tread results without the 300 m curve. It is possible to see that, without the 300 m curve, the standard-gauge wagon presents the highest values of $T\gamma$ and Wear Index (Fig. 10a and b). Furthermore, the standard-gauge wagon presents higher Wear depth values except for the 500 m curve, where it presents equivalent results with the broad-gauge. From the figure is also possible to see that the results from the standard-gauge wagon present a lower inclination when compared to the meter and broad-gauge. This result suggests that, as expected, the flange contact leads to higher creepages and hence higher values of the $T\gamma$ wear number. In fact, in the curves considered in Fig. 10a, the contact point is always on the tread for the Brazilian wagons, while the European wagon always features flange contact on the outer wheel. This can be related to the distinct types and stiffness of primary suspension on the European and Brazilian freight

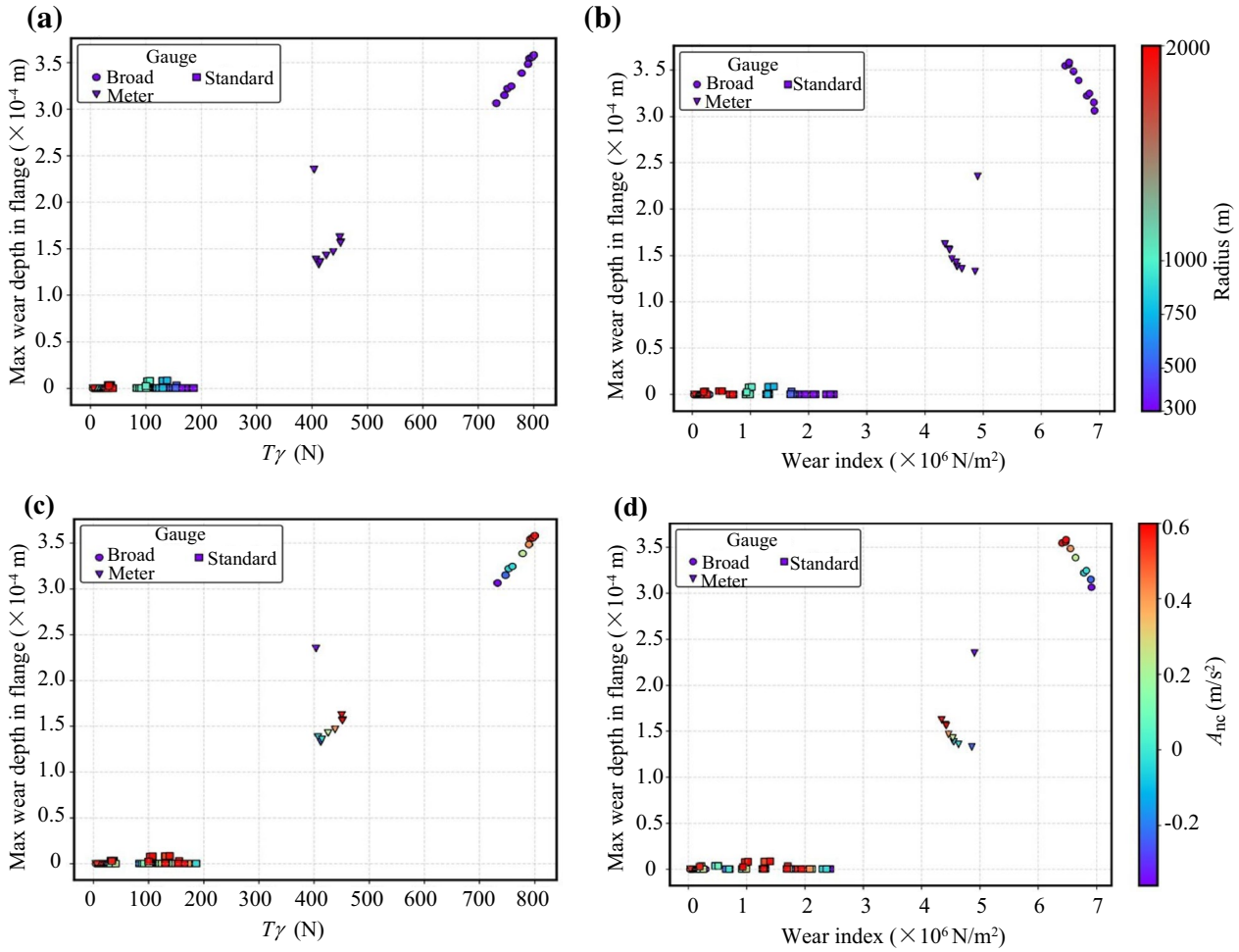


Fig. 9 Outer wheel wear depth on the flange: **a** by wear number and radius; **b** by wear index and radius; **c** by wear number and A_{nc}; **d** by wear index and A_{nc}

bogies. The primary suspension of the European Y25 bogie limits the yaw angle of the wheelset, thus leading to flange contact.

At the same time, the larger inclination of the data corresponding to the Brazilian wagons is due to the differences in the axle-load values of European and Brazilian wagons, since the wear volume is proportional to the normal load, as stated by Archard's law in Eq. (3). While the axle load of the Brazilian wagons is higher compared to the reference European wagon, similar values of $T\gamma$ are expected to lead to higher wear on the Brazilian wagons. Without the 300 m curve, it is not possible to distinguish a positive or negative correlation between $T\gamma$ and Wear depth, and Wear Index and Wear depth.

Figure 10c and d show the A_{nc} results. The same behavior observed in the results with the 300 m curve is shown by the standard-gauge wagon, i.e., the Wear depth increases as the A_{nc} decreases. Although, the same can not be said about the meter and broad gauge.

Figure 11 shows the outer wheel wear depth on the flange results without the 300 m curve. In this condition, only the standard gauge wagon presented flange wear. No correlation is observed for the wear depth and $T\gamma$, and wear depth and wear index (Fig. 11a and b). For the A_{nc} results (Fig. 10c and d) two different behaviors appear, for values of $T\gamma$ and wear index higher than 80 N and 0.75×10^6 N/m^2, respectively, the highest Wear depth occurred to the highest value of A_{nc}, 0.6m/s^2. For values under those, there is no clear correlation between A_{nc} and Wear depth. The reason for this absence of correlation can be better explained by a deeper analysis of the outputs obtained from the standard-gauge European wagon model. From Fig. 12, which shows the wear area on the flange as a function of the wear number on that position, most of the simulations feature low values of wear, with a wear area lower than 0.15×10^{-8} m^2. Only a few points are characterized by large wear areas, and they can be graphically split into three groups, numbered I, II, and III. Detailed data analysis highlighted that all points featuring

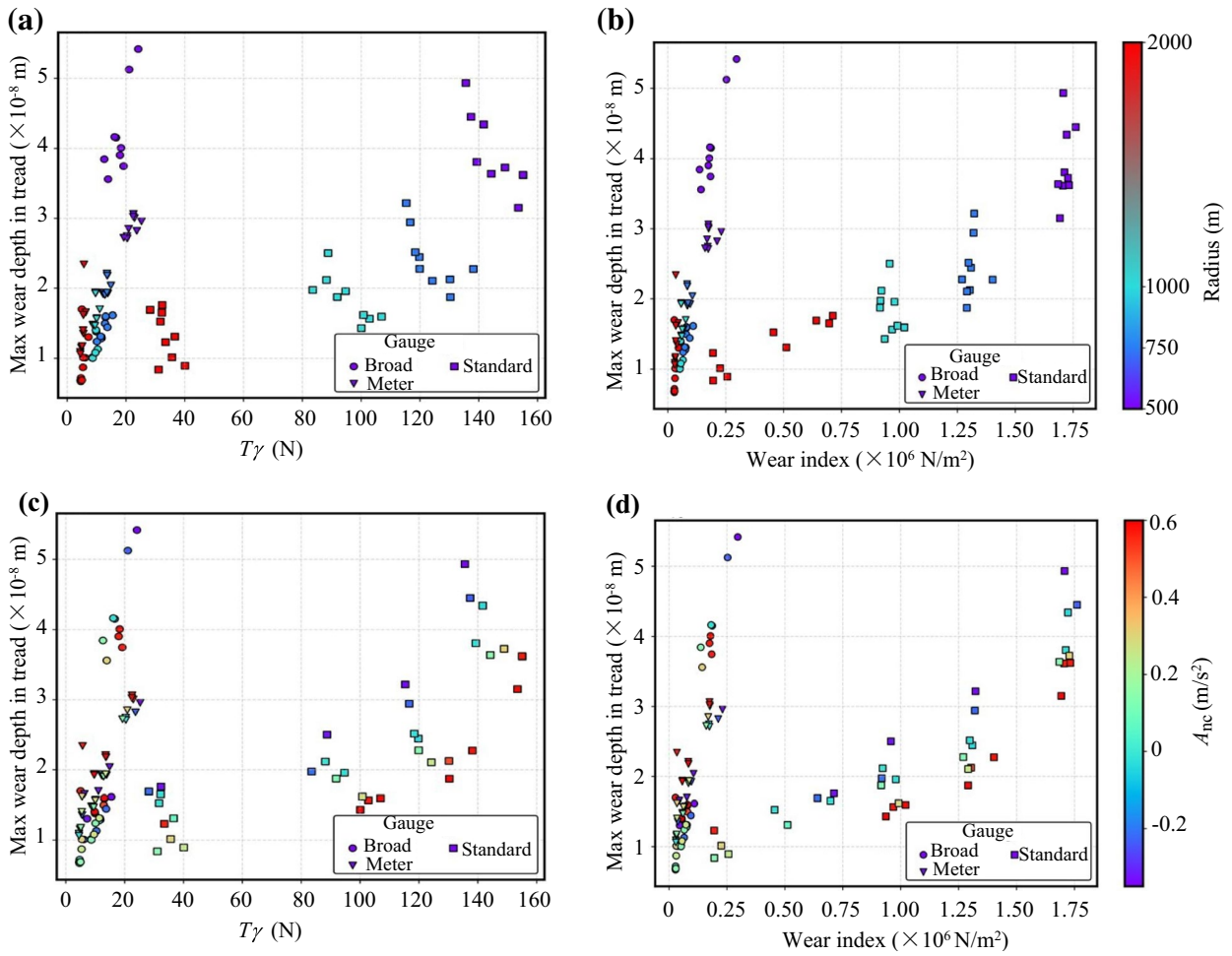


Fig. 10 Outer wheel wear depth on the tread without the 300 m radius curve: **a** by wear number and radius; **b** by wear index and radius; **c** by wear number and A_{nc}; **d** by wear index and A_{nc}

abnormal wear values correspond to large speed values for all curves with a radius of 500 m and above. In all these simulations, the slip speed on the outer wheel while negotiating the curves is above 0.2 m/s, which is the threshold causing entrance into the severe regime in Archard's map (see Fig. 2). Regarding data belonging to groups I and III, the slip speed is above the threshold value both in the entry and outlet transitions as well as in the full curve section.

Concerning the two simulations belonging to group II, the slip speed overcomes the threshold limit only in the entry and exit transitions, while the contact conditions correspond to the mild regime in the full curve section. Therefore, based on these observations, two regression lines were calculated, namely a regression line for the points belonging to the low wear group (mild regression line), and a second regression line for the points falling into groups I and III altogether (severe regression line). For both regression lines, the correlation factor is close to 1, with values above 0.97. The ratio of the slope of the severe regression line over the slope of the mild regression line is approximately equal to 21. This is in line with the ratio of the severe over mild wear coefficients, which is equal to 30. Therefore, it can be stated that the absence of a unique correlation for the output data is related to this bilinear behavior, as the combination of speed, radius, and superelevation may lead to severe wear. Nonetheless, when the wear regime is identified, a remarkably high correlation exists between wear number and worn material, as expected.

The results obtained for the Brazilian wagon do not show this peculiarity, because when the curve radius is equal to 500 m or greater the contact point is always on the tread, where the slip speed is far away from the values that would cause severe wear. This discrepancy is caused by the main differences between European and Brazilian wagons, as bogie types, wheel and rail profiles, and axle load.

Figure 13 shows the inner wheel wear depth on the tread results. In Fig. 13a, $T\gamma$ increases as the curve radius decreases. The Wear depth also increases with the decreasing

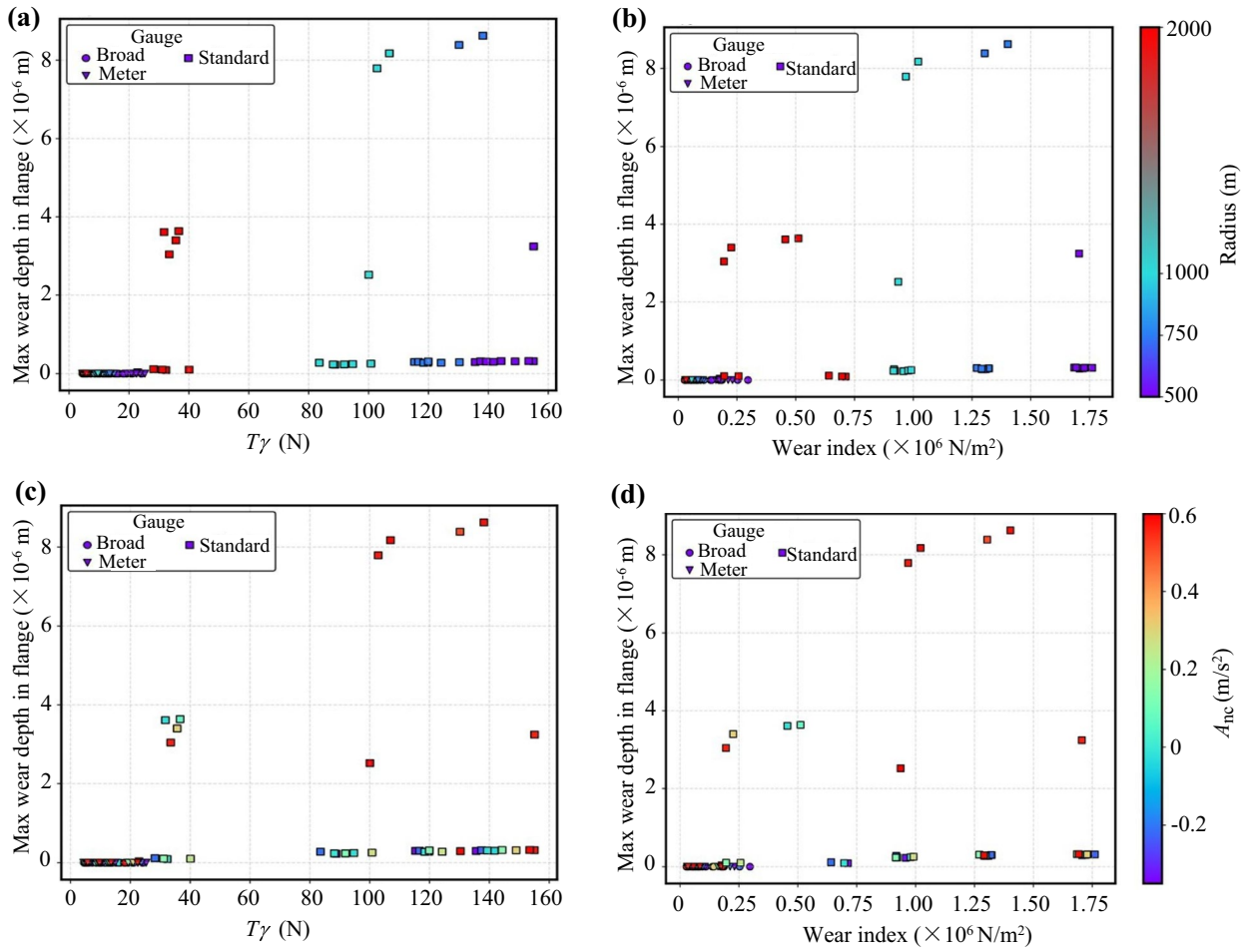


Fig. 11 Outer wheel wear depth on the flange without the 300 m radius curve: **a** by wear number and radius; **b** by wear index and radius; **c** by wear number and A_{nc}; **d** by wear index and A_{nc}

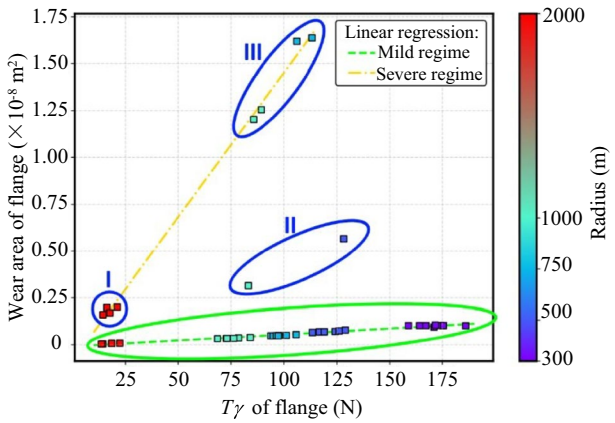


Fig. 12 Bilinear behavior of the outputs collected from the simulations run with the standard-gauge European wagon

in the curve radius. The higher values for $T\gamma$ are observed for the broad-gauge wagon, followed by the standard and then the meter gauge. Similarly, maximum wear depth values are observed for standard and meter gauge wagons. For the Wear Index a different behavior is observed (Fig. 13b), since the standard-gauge wagon presents the highest Wear Index values. This can indicate that the standard gauge wagon presents a smaller contact area. Furthermore, no correlation with the Wear depth is observed.

Figure 13c and d show the results by A_{nc}. In Fig. 13c there seems to be a small influence of the A_{nc} in the $T\gamma$ for the meter-gauge wagon, while for the other two, standard and broad-gauge, it seems to have a strong correlation, where a decrease in the A_{nc} increases the $T\gamma$ and wear index. A high negative influence in the wear depth is observed, i.e., an increase in the A_{nc} decreases the wear depth. For the wear index (Fig. 13d), only the broad gauge presents a correlation between wear index and A_{nc}. Furthermore, the same negative influence in the wear depth is observed for the wear index.

Figure 14 shows the inner wheel wear depth on the flange results. In Fig. 14a, the meter and broad-gauge for the 300 m curve radius presented much higher values of

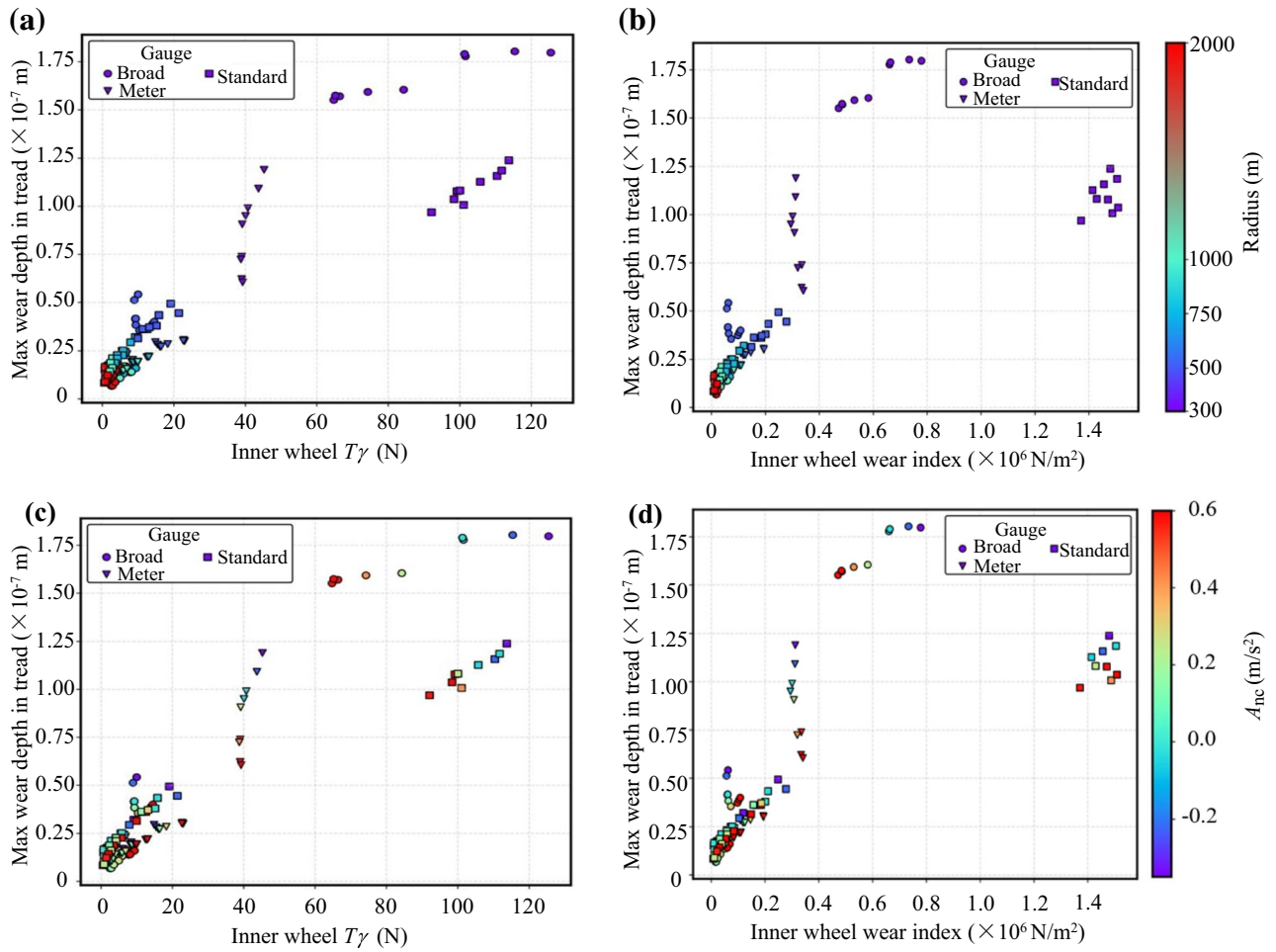


Fig. 13 Inner wheel wear depth on the tread: **a** by wear number and radius; **b** by wear index and radius; **c** by wear number and A_{nc}; **d** by wear index and A_{nc}

Wear depth than the other cases, as expected. It is not possible to perceive any correlation between the $T\gamma$ and the wear depth, except for the case of broad-gauge with 300 m of radius. For this case, the Wear depth decreases with the increase of the $T\gamma$. The same behavior is observed in the wear index (Fig. 14b).

In Fig. 14c, a negative correlation between the $T\gamma$ and the A_{nc} is found, i.e., as the A_{nc} decreases whilst the $T\gamma$ increases. No correlation is observed between the A_{nc} and wear index (Fig. 14d), and A_{nc} and Wear depth, except for the broad-gauge in the 300 m radius curve, where an increase in the A_{nc} is related to a decrease in the wear index and an increase in the wear depth.

As done for the outer wheel, we analyzed the results without the 300 m radius curve, (Figs. 15 and 16). Figure 15 shows the tread results. A negative correlation between the $T\gamma$ and the curve radius as well as a positive correlation between $T\gamma$ and Wear depth is observed in Fig. 15a. In Fig. 15b a negative correlation is also observed between the wear index and the curve radius. Furthermore, there seems to be a positive correlation between the Wear Index and Wear depth, except for the broad-gauge case.

From Fig. 15c and d it seems that the higher wear depths are related to the smallest values of A_{nc}, but no clear correlation can be observed. Besides that, no correlation is observed between the wear depth and the $T\gamma$, and the wear depth and wear index.

As shown for the outer wheel (Fig. 11), for the inner wheel only the standard gauge type presented flange wear (Fig. 16). From Fig. 16a and b, we observe a negative correlation between $T\gamma$ and curve radius, and between the wear index and the curve radius too. No correlation between wear depth and $T\gamma$, and wear depth and wear index are observed. Furthermore, no correlation with the A_{nc} is observed in Fig. 16c and d). It is important to remark that, also for the inner wheel, the points characterized by the

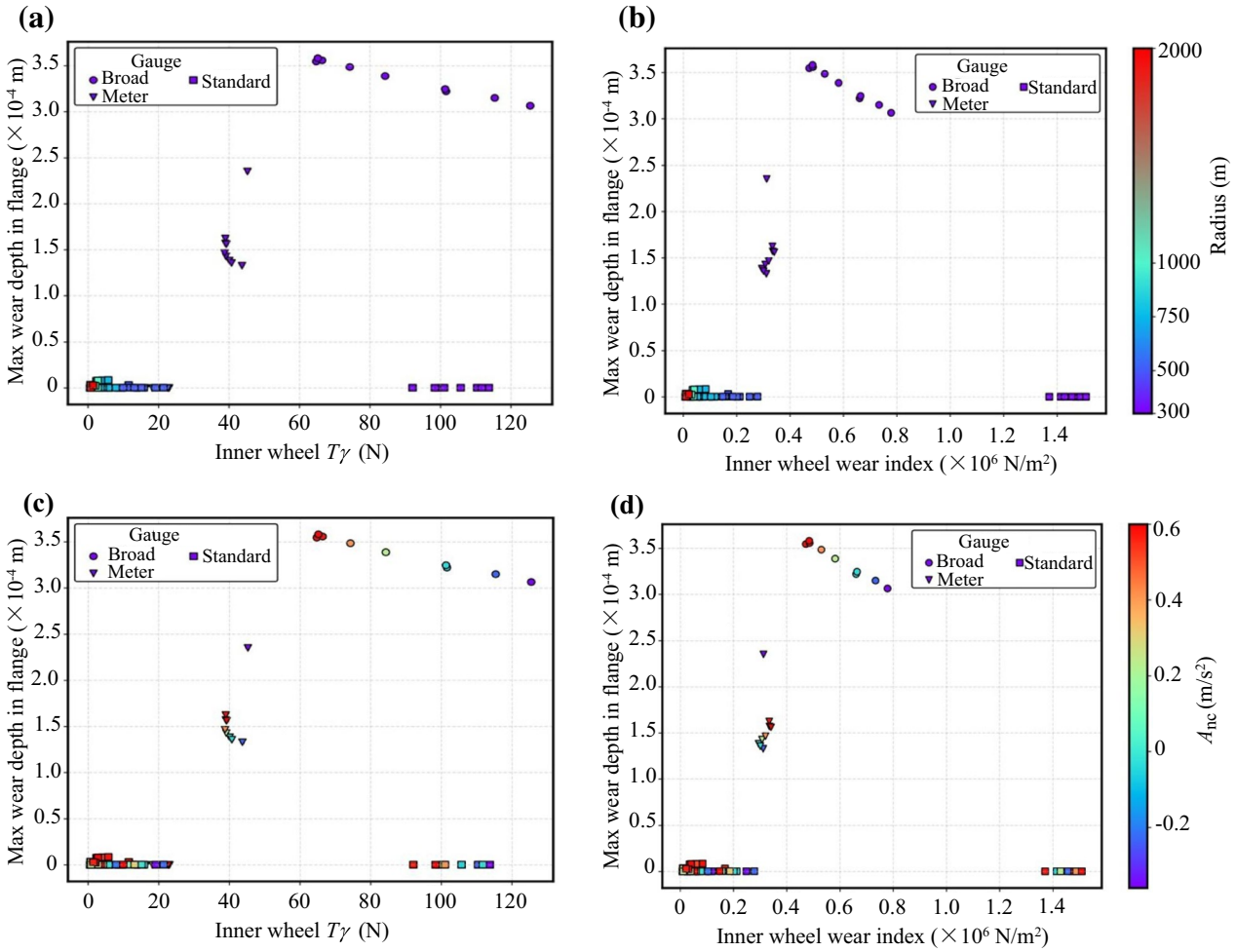


Fig. 14 Inner wheel wear depth on the flange: **a** by wear number and radius; **b** by wear index and radius; **c** by wear number and A_{nc}; **d** by wear index and A_{nc}

highest values of Wear depth (above 2 μm) correspond to the simulations featuring entrance in the severe regime of Archard's map on the outer wheel, see groups I, II and III in Fig. 12. If the outputs of these simulations are excluded, a good correlation still exists between worn material and the wear indexes.

4 Conclusions

In this paper, the $T\gamma$ and wear index derived from the vehicle-track model simulation are compared aiming to evaluate the effectiveness in quantifying wear on railway wheels, focusing on freight wagons, relying on two standard bogie architectures. The problem was approached by performing multibody dynamic simulations of three different wagons, two American bogies with meter and broad gauge, and a European bogie with standard gauge. The wagons were chosen to verify the generality of the results obtained. Different tracks, velocities, and superelevation were simulated. The main findings are as follows:

- Comparative results obtained from a performance simulation show for the outer wheel a remarkably high correlation (0.96) between $T\gamma$ and wear depth. This result indicates that the $T\gamma$ is better than the wear index to be used when analyzing wear depth. There is also a correlation of 0.82, between the wear index and wear area. In this way, the wear index was shown to be better than the $T\gamma$ for analyzing material lost through wear.

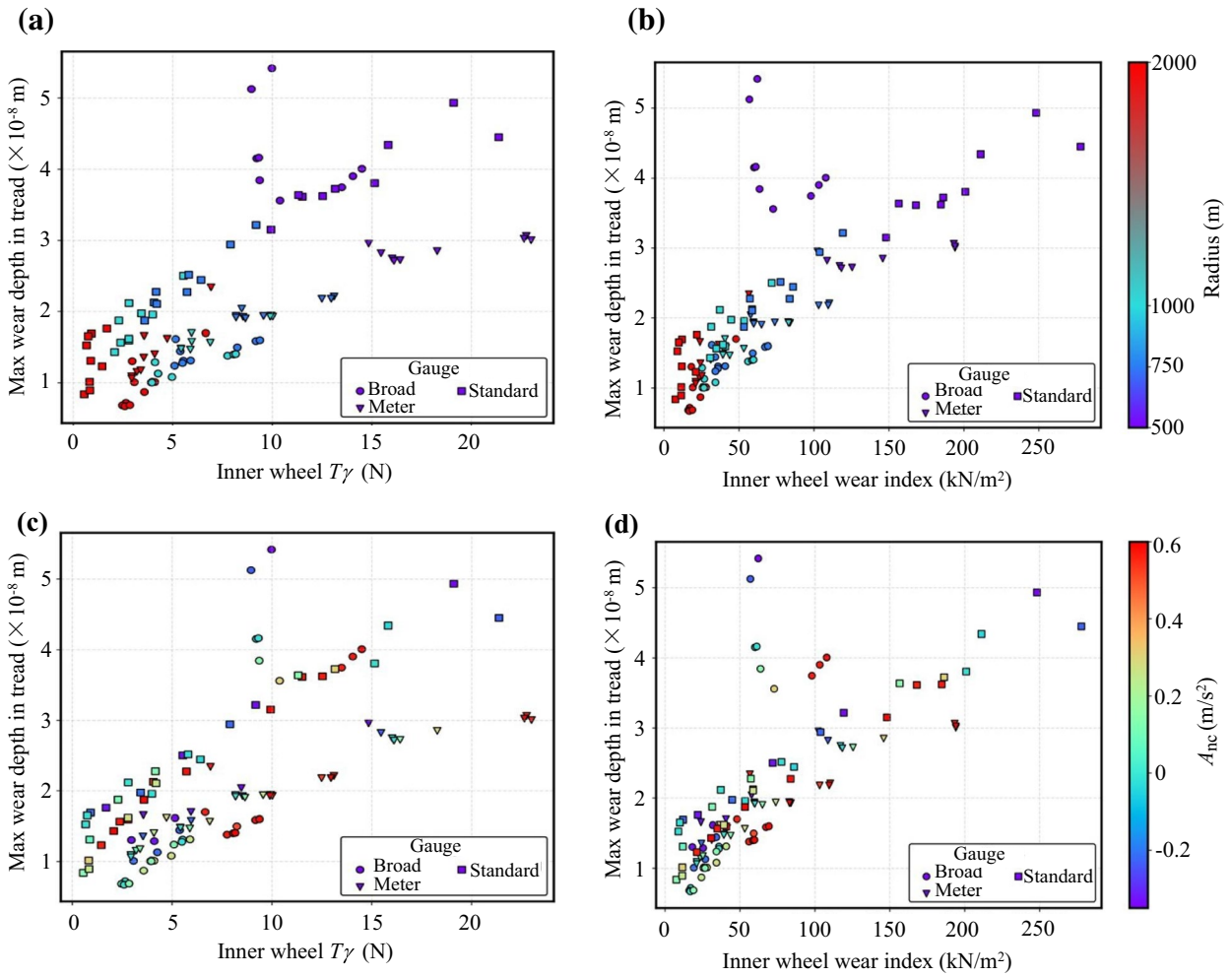


Fig. 15 Inner wheel wear depth on the tread without the 300 m radius curve: **a** by wear number and radius; **b** by wear index and radius; **c** by wear number and A_{nc}; **d** by wear index and A_n

- $T\gamma$ and wear index increases as the curve radius decreases. There seems to be a small influence of the A_{nc} on $T\gamma$ and wear index.
- Concerning the results including the 300 m radius curve, wear of the Brazilian wagons is larger with respect to wear of the European wagon. In fact, on the 300 m curve, flange contact occurs on the outer wheel of the Brazilian wagons, thus leading to a larger slip speed. Therefore, when similar contact conditions occur on European and Brazilian wagons, the wear produced on the Brazilian wagon is higher because of the larger axle-load values, since the wear volume is proportional to the normal load as stated by Archard's wear law equation.
- Based on the results for the flange excluding the 300 m curve, a lack of correlation for the European wagon is observed due to the combination of speed, radius, and superelevation that leads in some cases to severe wear. Nonetheless, when the wear regimes are used to classify the data, a remarkably high correlation exists between wear number and worn material, as expected. Brazilian wagons, however, do not show this peculiarity, because the contact point is always on the tread when the curve radius is 500 m or greater. The different behavior of the wagons can be mainly related to differences in wheel and rail profiles and differences in primary suspension between European and Brazilian freight bogies The European Y25 bogie has a primary suspension that limits the yaw angle of the wheelset, which contributes to flange contact.

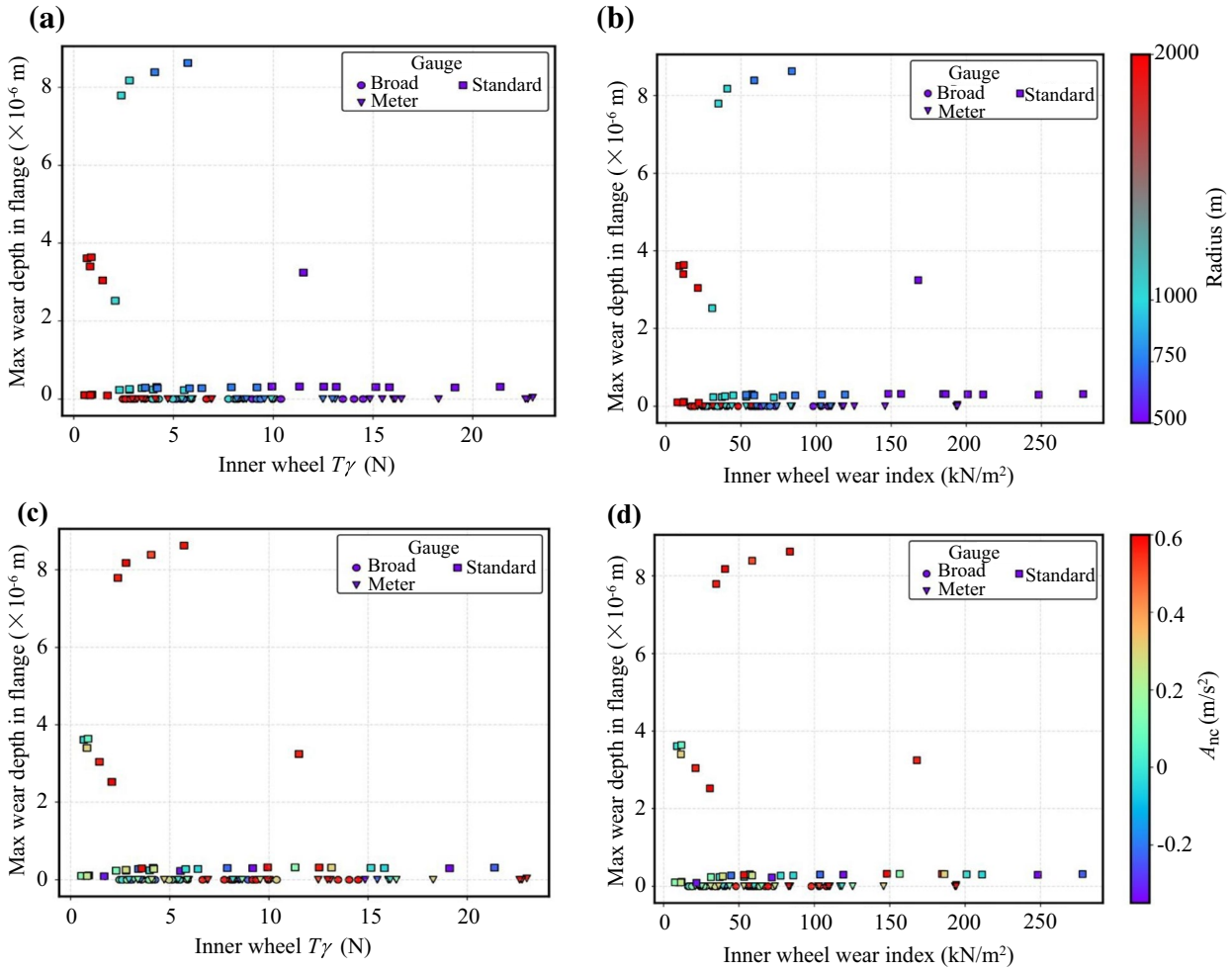


Fig. 16 Inner wheel wear depth on the flange without the 300 m radius curve: **a** by wear number and radius; **b** by wear index and radius; **c** by wear number and A_{nc}; **d** by wear index and A_{nc}

Finally, the findings of this work contribute to a better understanding of wheel wear and provide useful information for dynamic simulations, especially on its capacity of predicting wear. Based on the results of this study and the characteristics of the railway under study, the objective function for wheel optimization can be defined.

Acknowledgements The authors wish to express their acknowledgment to Vale S.A. for funding this study and technical support, and also to CNPQ (Grant Number 315304/2018-9) and CAPES (Grant Number 88887.892546/2023-00), which funded partially this project.

Open Access This article is licensed under a Creative Commons Attribution 4.0 International License, which permits use, sharing, adaptation, distribution and reproduction in any medium or format, as long as you give appropriate credit to the original author(s) and the source, provide a link to the Creative Commons licence, and indicate if changes were made. The images or other third party material in this article are included in the article's Creative Commons licence, unless indicated otherwise in a credit line to the material. If material is not included in the article's Creative Commons licence and your intended use is not permitted by statutory regulation or exceeds the permitted use, you will need to obtain permission directly from the copyright holder. To view a copy of this licence, visit http://creativecommons.org/licenses/by/4.0/.

References

1. Bernal E, Spiryagin M, Wu C et al (2023) iNEW method for experimental-numerical locomotive studies focused on rail wear prediction. Mechan Syst Signal Process 186:109898
2. Lewis R, Dwyer-Joyce RS, Olofsson U et al (2010) Mapping railway wheel material wear mechanisms and transitions. J Rail Rapid Transit 224(3):125–137
3. Bosso N, Magelli M, Zampieri N (2022) Simulation of wheel and rail profile wear: a review of numerical models. Railw Eng Sci 30(4):403–436
4. Ye Y, Qi Y, Shi D et al (2020) Rotary-scaling fine-tuning (RSFT) method for optimizing railway wheel profiles and its application to a locomotive. Railw Eng Sci 28(2):160–183
5. Hardwick C, Lewis R, Eadie D (2014) Wheel and rail wear—understanding the effects of water and grease. Wear 314(1–2):198–204

6. Elkins JA, Eickhoff BM (1982) Advances in non-linear wheel/rail force prediction methods and their validation. J Dyn Syst Meas Control 104(2):133–142
7. Sun Y, Spiryagin M, Cole C et al (2017) Wheel–rail wear investigation on a heavy haul balloon loop track through simulations of slow speed wagon dynamics. Transport 33(3):843–852
8. Krishna VV, Hossein-Nia S, Casanueva C et al (2022) Rail RCF damage quantification and comparison for different damage models. Railw Eng Sci 30(1):23–40
9. Santamaria J, Vadillo E, Oyarzabal O (2009) Wheel–rail wear index prediction considering multiple contact patches. Wear 267(5–8):1100–1104
10. Harvey RF, McEwen IJ (1986) The relationship between wear number and wheel/rail wear in the laboratory and the field. British Rail Research Report TM-VDY-001
11. Ye Y, Hecht M (2022) Wear concentration index: an alternative to the target T-gamma in railway wheel profile optimization. In: Orlova A, Cole D (eds) Advances in dynamics of vehicles on roads and tracks II. IAVSD 2021. Lecture notes in mechanical engineering. Springer, Cham
12. Pacheco PADP, Endlich CS, Vieira KLS et al (2023) Optimization of heavy haul railway wheel profile based on rolling contact fatigue and wear performance. Wear 522:204704
13. Ignesti M, Innocenti A, Marini L et al (2013) Development of a wear model for the wheel profile optimisation on railway vehicles. Veh Syst Dyn 51(9):1363–1402
14. Montenegro PA, Calçada R (2023) Wheel–rail contact model for railway vehicle–structure interaction applications: development and validation. Railw Eng Sci 31(3):181–206
15. Archard J (1953) Contact and rubbing of flat surfaces. J Appl Phys 24(8):981–988
16. Du G, Han F, Fan X, Li Y et al (2021) Dynamic simulation analysis of rail track and track structure based on SIMPACK and ABAQUS. Web of Conf 248:03007
17. Ayasse JB, Chollet H (2005) Determination of the wheel rail contact patch in semi-Hertzian conditions. Veh Syst Dyn 43(3):161–172
18. SIMPACK, About rail–wheel Pairs. In simpack user assistance, dassault systemes simula corp., 2022.
19. Corrêa PHA, Ramos PG, Fernandes R et al (2023) Effect of primary suspension and friction wedge maintenance. Wear 524–525:204748
20. Pacheco P, Reis T, Ramos P et al (2023) Wear and fatigue-oriented wheel profile optimized for heavy haul. VI Simpósio de Engenharia Ferroviária, Campinas
21. Pacheco P, Correa PHA, Ramos PG et al (2023) Effect of transition functions on the dynamic behavior of heavy-haul wagons. In: 20th International Wheelset Congress, Chicago
22. Pacheco P, Lopes M, Correa P et al (2023) Influence of primary suspension parameters on the wear behaviour of heavy-haul railway wheels using multibody simulation. In: Proc. of the International Conference on Electrical, Computer, Communications and Mechatronics Engineering, Tenerife, pp 1–5
23. Ramos P, Correa P, Texeira L et al (2022) Dynamic effect of hollow-worn wheels for freight rail vehicles in a consist. In: Proceedings of the 5th International Conference on Railway Technology: Research, Development and Maintenance. Montpellier, civil-comp conferences, Vol 1, Paper 21.4
24. Bosso N, Magelli M, Zampieri N (2023) Dynamical effects of the increase of the axle load on european freight railway vehicles. Appl Sci 13(3):1318
25. Lima EA, Baruffaldi LB, Manetti JLB et al (2022) Effect of truck shear pads on the dynamic behaviour of heavy haul railway cars. Veh Syst Dyn 60(4):1188–1208
26. Roviraa A, Roda A, Marshall MB et al (2011) Experimental and numerical modelling of wheel–rail contact and wear. Wear 271(5–6):911–924
27. Lewisand R, Dwyer-Joyce RS (2004) Wear mechanisms and transitions in railway wheel steels. Proc Inst Mech Eng Part J J Eng Tribol 218(6):467–478
28. Lewis R, Braghin F, Ward A et al (2003) Integrating dynamics and wear modelling to predict railway wheel profile evolution. In: 6th international conference on contact mechanics and wear of rail/wheel systems, Gothenburg.
29. Liu B, Bruni S, Lewis R (2022) Numerical calculation of wear in rolling contact based on the Archard equation: effect of contact parameters and consideration of uncertainties. Wear 490–491:204188
30. Jendel T (2002) Prediction of wheel profile wear—comparisons with field measurements. Wear 253(1–2):89–99
31. Lewis R, Olofsson U (2004) Mapping rail wear regimes and transitions. Wear 257(7–8):721–729
32. Bosso N, Magelli M, Zampieri N (2022) Study on the influence of the modelling strategy in the calculation of the worn profile of railway wheels. WIT Trans Built Environ 213:65–76
33. Associação Brasileira de Normas Técnicas (2019) NBR 16810: Via férrea—Superelevação em curvas
34. Rete Ferroviaria Italiana (2016) Prefazione generale all'orario di servizio in uso sulla infrastruttura ferroviaria nazionale per i convogli di RFI. Specification 15/2016
35. European Committee for Standardization (2006) Railway applications–wheelsets and bogies–wheels–tread profile, EN 13715:2006
36. Association of American Railroads (2011) Wheels, carbon steel specification M-107/M-208
37. Kuka N, Verardi R, Ariaudo C et al (2018) Impact of maintenance conditions of vehicle components on the vehicle–track interaction loads. Proc Inst Mech Eng Part C J Mechan Eng Sci 232(15):2626–2641
38. Benesty J, Chen J, Huang Y et al (2009) Noise reduction in speech processing. Springer, Berlin, Heidelberg
39. Ratner B (2009) The correlation coefficient: Its values range between +1/−1, or do they? J Target Meas Anal Mark 17:139–142
40. Shevtsov I, Markine V, Esveld C (2006) Optimal design of wheel profile for railway vehicles. Wear 258(7–8):1022–1030